

Multiscale Modeling of Drug–Polymer Nanoparticle Assembly Identifies Parameters Influencing Drug Encapsulation Efficiency

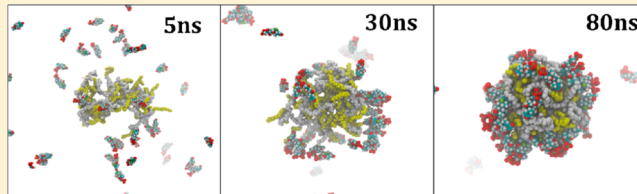
R. Mackenzie,[†] J. Booth,[‡] C. Alexander,[§] M. C. Garnett,[§] and C. A. Laughton*,[†]

[†]Division of Medicinal Chemistry & Structural Biology, [§]Division of Drug Delivery & Tissue Engineering, School of Pharmacy, University of Nottingham, Nottingham NG7 2RD, United Kingdom

[‡]Pharmaceutical Development, AstraZeneca, Macclesfield SK10 2NA, United Kingdom

Supporting Information

ABSTRACT: Using a multiscale (dual resolution) approach combining an atomistic (GROMOS96) and coarse-grain (MARTINI) force field, we have been able to simulate the process of drug–polymer nanoparticle assembly by nanoprecipitation from mixed solvents. Here, we present the development and application of this method to the interaction of three poly(glycerol adipate) polymer variants with the anticancer drug dexamethasone phosphate. Differences in encapsulation efficiency and drug loading between the polymers are in agreement with the experimental trend. Reference atomistic simulations at key points along the predicted aggregation pathway support the accuracy of the much more computationally efficient multiscale methodology.



INTRODUCTION

There is an increasing interest in nanomedicines due to the way that nanoparticles are handled physiologically within the body. Compared to conventional formulations, nanoparticles provide opportunities to exploit different barriers and uptake mechanisms to treat difficult diseases such as cancer and parasitic infections.² Research and development related to drug delivery technology is therefore becoming increasingly important for the pharmaceutical industry. Methodologies for encapsulation of drugs into micro- and nanoparticles for use as drug delivery systems have been under development for at least 2 decades. A variety of different types of materials are used for drug encapsulation, but they are mainly divided into lipid-based technologies, such as liposomes or solid lipid nanoparticles, and polymer-based methodologies.³ There are examples of liposome-based nanoparticles that have been in clinical use for several years. However, although drug encapsulation within polymeric nanoparticles has been achieved for a variety of polymers and small molecule drugs,^{4–10} it is only recently that the first polymer-based nanoparticle became clinically available.³ This is important because the mechanisms of drug incorporation for the former are relatively easy to appreciate, but there is not a clearly understood mechanism for drug incorporation in the latter. It is these polymer based technologies that are of interest in this article.

There are a number of established methods for the production of nanoparticles and incorporation of drugs.¹¹ Some of these processes have been investigated and analyzed from a physicochemical viewpoint,¹² but they have not been modeled at a detailed level. Many of the nanoparticles produced have poor incorporation of drug and rapid drug release rates, where most delivery applications require high

drug incorporation and slow release rates. Currently, improvements in encapsulation are dependent largely on trial and error to improve methodology and to introduce materials and excipients with different properties that may be beneficial for nanoparticle performance. Part of the problem with polymer nanoparticles is that we need to use processes that will both create the nanoparticle and simultaneously facilitate the incorporation of drug into that nanoparticle. The mechanisms of both of these aspects are poorly understood at a molecular level.

Molecular simulation methods have the potential to provide insight into the fundamental processes at the atomic level that govern the emergent properties of a complex system on the macroscopic scale. However, until recently, the computational expense of applying such techniques to the study of drug–polymer interactions has limited its application.^{13,14} Samanta et al. have analyzed the interactions of a single drug molecule with a few polymer chains,¹⁵ and Ahmad et al. have simulated 20 drug molecules with 8 polymer chains in a single solvent.¹⁶ Other papers have taken a mesoscale approach to modeling the polymers using dissipative particle dynamics.^{17,18} This allows for the simulation of larger structures such as polymersomes,¹⁹ but, as these methods do not deal with the system on the atomic scale, they (a) limit our ability to draw on our understanding of the basic chemistry of intermolecular interactions to explain and predict behavior and (b) limit the metrics that can be extracted from such simulations for comparison with experimental observables, such as spectroscopic properties.

Received: December 19, 2014

Published: May 13, 2015

In the light of ever-increasing computational power and new developments in simulation methods, it is timely to tackle this problem. We have chosen one particular drug–polymer assembly process, namely, nanoprecipitation, which is widely used for nanoparticle preparation.⁸ In this method, droplets of a water-insoluble polymer in a water-miscible organic solvent were added to a large excess of water. Drug can either be present in the organic polymer solution or the aqueous receiving solution, depending on the drug's properties. We have previously published work where the drug dexamethasone phosphate (DXMP) has been encapsulated into polymers based on poly(glycerol adipate) (PGA). PGA is synthesized using an enzymic method to produce a functionalized biodegradable polymer bearing pendant hydroxyl groups.⁹ PGA may be flexibly modified by functionalization of some or all of its free hydroxyl groups to produce polymers with different physicochemical properties.^{7,9} We have demonstrated that drug loading of DXMP into PGA is affected by polymer molecular weight and functionalization by acylation (both acyl chain length and percentage acylation). A partial functionalization by stearate (C18) was most effective for drug loading. The physicochemical rationalization for these data is not obvious. While steroids such as cholesterol are known to intercalate with acyl lipid chains in biological membranes, the details of why and how a relatively polar steroid drug is encapsulated efficiently into a very hydrophobic polymer by the nanoprecipitation method are not obvious.

Conceptually, nanoprecipitation involves a number of processes that will be somewhat interdependent in a complex way. First, there is the solvent diffusion process, whereby the water-miscible organic solvent disperses into bulk water and water enters into the volume of the original droplet. This change in the solvent environment of the (hydrophobic) polymer triggers other processes, such as a change in the polymer chains from an extended to a compacted conformation, intramolecular collapse, intramolecular aggregation, and polymer chain entanglement. At the same time, the drug molecules will be diffusing into the region around the polymer in response to a concentration gradient, modulated by their affinity for the various species present.

Nanoprecipitation has been modeled previously by Spaeth et al. using a single solvent type whose interaction parameters with the solutes were changed during the simulation to recreate the dispersion of acetone.²⁰ Some preliminary simulations we performed suggested that this method has some drawbacks, as the absence of a water/acetone solvent gradient across the simulated system changes its behavior. Here, we describe the development and application of a multiscale modeling method that explicitly includes this process. We find that by treating solvent–solvent and solvent–solute interactions in a coarse-grained manner, while maintaining atomistic resolution in modeling solute–solute interactions, we can achieve a balance between computational speed and accuracy (as benchmarked against fully atomistic simulations). This modeling investigates and recapitulates the established trends in the experimental data, and, in the process, it gives detailed insights into some of the factors, on the atomic scale, that influence encapsulation efficiency.

METHODS

Polymer Designations. The unmodified polymer is designated simply PGA₁₀₀. Acylation of the pendant hydroxyl

group with stearyl moieties is designated C18PGA, with a subscript used to denote the percentage of monomers modified.

Multiscale Model. Our aim has been to model the time evolution of a system that begins as a spherical drop of a PGA polymer solution in acetone within a large box of water containing DXMP. To mimic the previously reported experimental conditions,^{7,9} we calculated that a suitable fully atomistic model that contained all of the relevant species would consist of a 12 nm diameter droplet containing 16 000 molecules of acetone and two molecules of a PGA₁₀₀ 30mer (or one molecule of PGA₂₀-*co*-C18PGA₈₀ or C18PGA₁₀₀ 30mer) at the center of a 60 nm³ box of ca. 7 million molecules of water and 1270 molecules of DXMP. In total, this would consist of over 21 million atoms. Such a system would be at the limits of what is practical to simulate on even Tier0 computational resources and yet would contain only a single molecule of C18PGA₁₀₀ polymer. To include more polymer molecules, we would need a larger droplet of the organic solvent and a larger box of water to surround it.

To address these issues, we have taken advantage of the facility in the MD code GROMACS²¹ to use multiscale, dual-resolution modeling methods. Water and acetone have been modeled as purely coarse-grained entities, using the MARTINI model and parameters.²² PGA and DXMP were modeled at both atomistic and coarse-grained levels, using the virtual sites approach.^{23,24} Thus, in our simulations, all solute–solute interactions are treated fully atomistically, but solute–solvent and solvent–solvent interactions are treated using a coarse-grain force approach. While the modeled concentration of the drug in water is comparable to experiment at 3.22 mg/mL, we have decreased the amount of acetone present in the system while increasing the polymer concentration to about four times the experimental value. This allowed us to observe how multiple polymer chains interact together to form a nanoparticle on a reasonable time scale (around 5 days on 192 cores). Increased concentrations were also used in similar work by Spaeth et al.²⁰ Overall, we have thus been able to reduce the number of particles in the simulation system to 1 054 063 for two PGA₂₀-*co*-C18PGA₈₀ chains and 1 053 653 for three PGA₁₀₀ chains with 500 molecules of DXMP.

Atomistic models, compatible with the GROMOS96 53a6²⁵ force field, for PGA, C18PGA, and DXMP were generated using the automated topology builder (ATB).²⁶ PGA₁₀₀ consists of 30 PGA monomers and PGA₂₀-*co*-C18PGA₈₀ consists of 4 PGA monomers with 26 C18PGA monomers evenly distributed throughout the polymer.

For the MARTINI force field,²² the polymer has been modeled with 4 coarse-grain (CG) sites per monomer. DXMP is modeled as 9 CG sites because ring structures require a 3 to 1 or lower mapping. The CG beads were mapped on to the atomistic coordinates using VOTCA²⁷ and converted to virtual sites.

As per the standard MARTINI approach, four water molecules are represented by a single water bead and a single acetone molecule is represented by a single acetone bead. Details of the mapping and all nonstandard parameters for the simulations are reported in the Supporting Information.

Simulation Parameters. GROMACS, version 4.6, was used for all production molecular dynamics. Simulations used periodic boundary conditions with Coulomb and van der Waals interactions shifted between 0 and the 1.2 nm cutoff. The Berendsen barostat and v-rescale thermostat were used to equilibrate the system to 1 bar, 300 K before a constant volume

production run. Bonds were constrained using the LINCS algorithm to allow for a 2 fs time step. Simulations were run for 80 ns, with coordinates saved every 100 ps. All simulations were repeated three times, starting from different, randomized initial velocity distributions.

Resolution Transformation. As part of the simulation validation procedure (discussed below), at various points, 11 nm³ subsections of the 50 nm³ multiscale systems were converted back to fully atomistic representations. We used the backward Python script²⁸ to reintroduce atomistic detail to our coarse-grain solvent. Atomistic molecules (one for acetone and four for water) are placed in position of coarse-grain beads and subjected to energy minimization and iterative molecular dynamics simulations with an increasing time step up to 2 fs. The original polymer and drug molecules with counterions were reintroduced to the simulation box without their coarse-grain virtual sites to create a fully atomistic subsystem.

Comparative Analysis of Multiscale and Atomistic Simulations. Fully atomistic MD on these subsystems was run for 5 ns using the GROMOS96 53a6 force field. A 2 fs time step was used with all bonds constrained. Temperature and pressure were kept constant at 300 K and 1 bar with the v-rescale thermostat and Berendsen barostat, respectively. The particle mesh Ewald method was used for Coulomb interactions with a 1.2 nm cutoff, and van der Waals interactions were cutoff at 1.2 nm. For comparison, each 11 nm³ subsection was also simulated for 5 ns using the multiscale force field.

The performance of the multiscale simulation vis-à-vis the atomistic gold standard MD was analyzed with regard to two key parameters. First, the time evolution of the total radius of gyration of the polymer clusters in the two simulations was compared using *g_gyrate*, and the autocorrelation function for this metric was calculated using *g_analyze*.

Second, the average orientation of the absorbed DXMP molecules with respect to the polymer nanoparticle was evaluated. For this, we measured the difference in the distance of the phosphate and O3 oxygen atoms of DXMP from the polymer cluster center of mass over the course of the simulation using *g_dist* (Figure 1). This was repeated for five different (randomly selected by number) drug molecules and averaged. In addition, the radial distribution of all DXMP molecules from the center of mass of the polymer nanoparticle was calculated over the last 30 ns of the simulation using *g_rdf*.

Calculation of Drug Loading and Encapsulation Efficiency. Experimentally, polymer-based drug delivery systems are analyzed for their ability to encapsulate drug molecules. There are a variety of experimental techniques used to discern the amount of drug that is encapsulated. For our simulations, we have the luxury of being able to see exactly how many drug molecules make contact with the polymer nanoparticle when it has formed.

The two most commonly used metrics for measuring drug encapsulation are encapsulation efficiency (EE) (eq 1.1) and drug loading (DL) (eq 1.2). Encapsulation efficiency will give an indication as to the amount of drug that was present in solution that ends up encapsulated in the polymer nanoparticle. This value depends on the amount of drug present at the start of the simulation. If a small amount of drug was present in solution and it eventually all gets encapsulated on the surface of the polymer, then the EE is 100%. As such, it can give values that may not give an accurate indication of the encapsulation ability of a polymer.

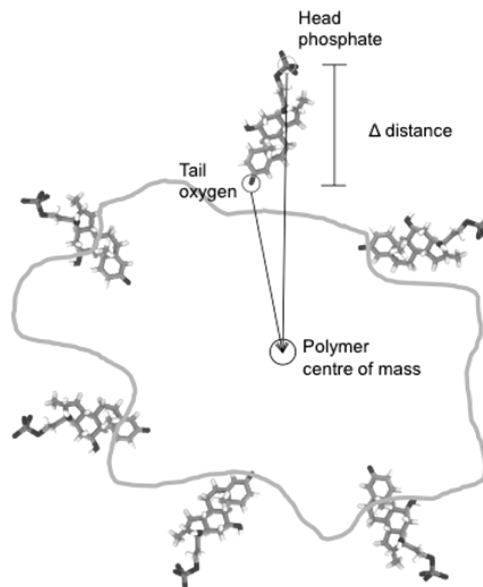


Figure 1. Calculation of the orientational metric (Δ distance).

To alleviate this problem, the DL is also calculated. DL is an indication of the total capacity for a polymer nanoparticle to encapsulate drug molecules. Ideally, this value should be as large as possible to get the optimal delivery of drug from the polymer nanoparticle. However, DL is often very low for polymer-based drug delivery systems. EE for a polymer could be 100%, yet the DL may still be low, depending on the amount of drug present in solution at the start. In our simulations, a drug was considered to be bound to the nanoparticle if it made contact with it.

$$\text{encapsulation efficiency} = \frac{\text{mass of drug in nanoparticle}}{\text{total mass of drug used}} \quad (1.1)$$

$$\text{drug loading} = \frac{\text{mass of drug in nanoparticle}}{\text{total mass of nanoparticle}} \quad (1.2)$$

RESULTS AND DISCUSSION

Optimisation/Calibration of the Multiscale Model. The relative dielectric constant (ϵ_r) must be carefully chosen for any multiscale simulation. The ϵ_r specifies the strength of electrostatic interactions between molecules in the system, with high values of ϵ_r resulting in increased dampening of Coulombic forces. The MARTINI force field is designed to use $\epsilon_r = 15$; however, the GROMOS96 53a6 atomistic force field is calibrated to a value of 1. This results in a conundrum for the multiscale model, which uses both force fields but must select one value of ϵ_r for the whole simulation. After extensive test runs, we found that, with careful adjustment of the nonbonded CG virtual site interactions with the solvent molecules, excellent agreement between multiscale and reference atomistic simulations could be achieved using $\epsilon_r = 6$ for the former. The effect of ϵ_r on simulation behavior is discussed in more detail below.

The MARTINI force field claims a 3–8 effective speed up over atomistic simulations,²² mainly due to the loss of effective friction when using CG beads. To ensure that the rate of acetone dispersion, and subsequently the rate of polymer nanoprecipitation, was correct in the multiscale simulations, we

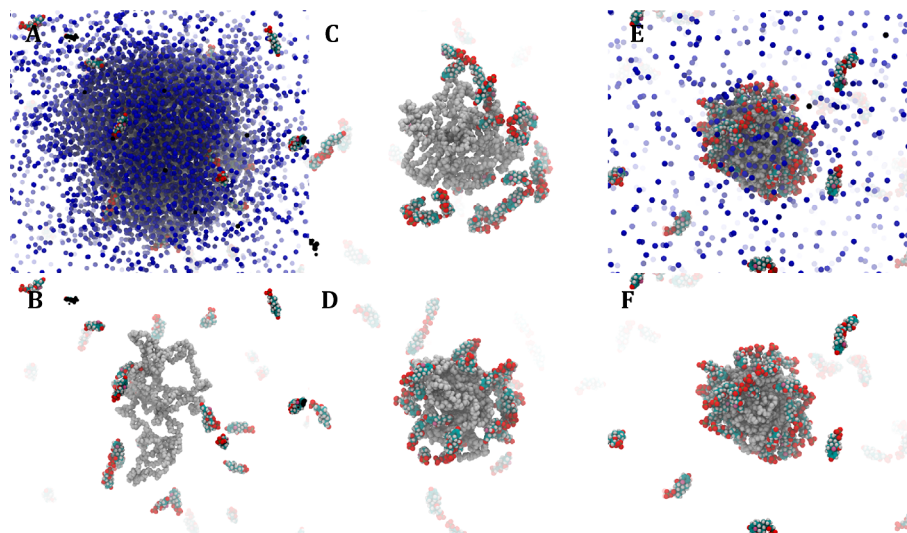


Figure 2. Snapshots taken during the 80 ns multiscale simulation of PGA_{100} with DXMP: (A) 5 ns (with acetone shown), (B) 5 ns, (C) 30 ns, (D) 50 ns, (E) 80 ns (with acetone shown), and (F) 80 ns. DXMP (multi), PGA (white), acetone (blue). For clarity, water and coarse-grain virtual sites are not shown.

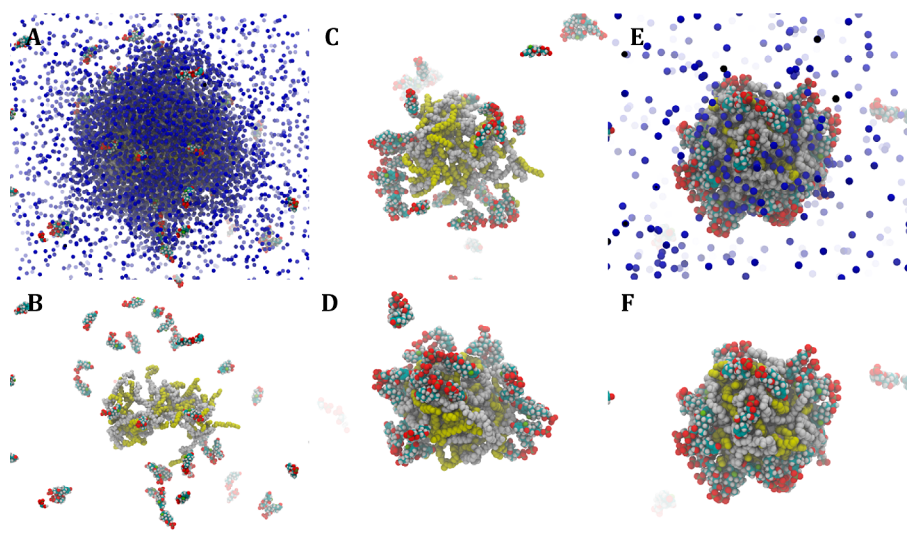


Figure 3. Snapshots taken during the 80 ns multiscale simulation of $\text{PGA}_{20}\text{-co-}\text{C18}\text{PGA}_{80}$ with DXMP: (A) 5 ns (with acetone shown), (B) 5 ns, (C) 30 ns, (D) 50 ns, (E) 80 ns (with acetone shown), and (F) 80 ns. DXMP (multi), PGA (white with C18 chains yellow), acetone (blue). For clarity, water and coarse-grain virtual sites are not shown.

carried out test MD simulations. Atomistic and coarse-grained models on mixed acetone/water systems showed that default MARTINI parameters underestimate the acetone diffusion coefficient ($1.367 \times 10^{-5} \text{ cm}^2/\text{s}$ by the Einstein relation, compared to $2.113 \times 10^{-5} \text{ cm}^2/\text{s}$ for the atomistic simulation). This contradicts the expected speed up in dynamics for CG molecules over their atomistic equivalents. Adjustments to the solvent intermolecular potentials (see the Supporting Information) resulted in excellent agreement with the atomistic diffusion coefficient ($2.213 \times 10^{-5} \text{ cm}^2/\text{s}$ for the multiscale system).

Simulation of PGA_{100} Nanoprecipitation in the Presence of DXMP. Using the simulation setup in the Methods section (a droplet of a polymer in acetone solution within a box of an aqueous solution of DXMP), we first explored the nanoprecipitation of the parent, unsubstituted PGA_{100} over an 80 ns multiscale simulation. The polymer

molecules in the acetone drop at the beginning of the simulation are initially well-dispersed and in chain-extended conformations (Figure 3B). As the acetone disperses into the surrounding water, the relatively hydrophobic polymer chains move toward the center of the shrinking droplet. Because the rate of diffusion of the polymer chains is slower than that of the solvents, they experience an increasingly polar environment and polymer–polymer interactions become more prominent. This produces both intramolecular collapse of individual polymer chains and stronger, more entangled intermolecular interactions. DXMP binds to the polymer at the surface of the acetone drop as PGA_{100} is exposed in these regions to the surrounding water. Eventually, enough acetone disperses to cause full aggregation of the polymer chains; at this point, a proportion of DXMP molecules becomes encapsulated in the nascent nanoparticle (Figure 2D–F).

Many of the features of this simulation are critically dependent on the nature and kinetics of the solvent exchange and dispersion process. It was originally assumed that acetone–water equilibration of the droplet happens instantaneously, compared with polymer–polymer dynamics, preventing the need to simulate acetone dispersion. However, in preliminary simulations beginning with dispersed and extended polymer chains in pure water, polymer chains tended to undergo intramolecular collapse much more rapidly than intermolecular aggregation, producing a very different form of granular material (results not shown). Simulations using a single solvent type whose characteristics were morphed, with properties ranging from pure acetone to pure water over the course of the simulation, in a manner similar to Spaeth et al.,²¹ also produced much less entangled structures because there is no retreating acetone/water interface to drive association (results not shown).

Simulation of PGA₂₀-co-C18PGA₈₀ Nanoprecipitation in the Presence of DXMP. The aggregation of the PGA₂₀-co-C18PGA₈₀ polymer chains is subtly different from that of the parent, unfunctionalized PGA. The more hydrophobic carbon chains are sparingly soluble in acetone and are free to extend away from the polymer (Figure 3C). Toward the end of the simulation, the polymer chains become more exposed to the water-rich environment, resulting in the carbon chains becoming buried in the emerging nanoparticle (Figure 3D–F). However, due to the degree of side-chain functionalization of this polymer, there is insufficient PGA backbone to fully shield the hydrophobic C18 chains from the surrounding water. This leaves hydrophobic chains exposed to interact with DXMP molecules at the surface (Figure 3F).

Similarly to the PGA₁₀₀ simulation, DXMP molecules that diffuse into the nascent nanoparticle bury their more hydrophobic groups in the C18/acetone phase, keeping the hydrophilic phosphate group in the polar PGA backbone/aqueous phase (Figure 3).

In practical formulation experiments, DXMP-loaded nanoparticles were found to display a 20% larger zeta potential than that of nonloaded polymer nanoparticles.⁵ This finding is one indication that the simulation is consistent with wet-lab data and suggests the orientational preference of DXMP seen in these simulations, i.e., with the exposed phosphate groups at the surface of the nanoparticles, is a plausible explanation for the observed negative zeta potential in the experimental nanoparticles.

Model Validation. To assess the accuracy of our multiscale simulations, a single fully atomistic simulation of the nanoprecipitation of the polymer was run and the aggregation of the polymer chains was compared with the behavior observed using the multiscale force field (Figure 4). In general, the agreement is excellent, although R_g decreases slightly faster using our multiscale force field and in addition the final nanoparticle is denser using the fully atomistic (GROMOS96) force field. This appears to be due to CG acetone lubricating polymer chains in the multiscale nanoparticle and so decreasing the particle's density.

Repeating all simulations at the fully atomistic level was computationally too costly; therefore, to further compare these force fields, snapshots of manageable but representative subsections of the whole simulation system, centered on the nascent nanoparticle, were extracted at three time points (30, 50, and 80 ns) from each multiscale simulation. We then used a procedure originally developed for multiscale biomolecular

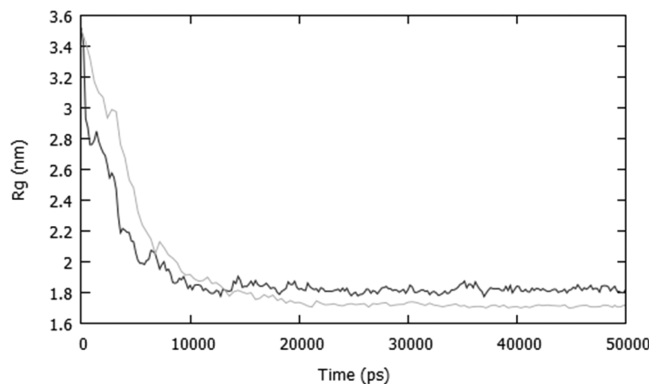


Figure 4. Total radius of gyration for a two-polymer cluster over a 50 ns nanoprecipitation simulation performed using a fully atomistic (light gray) or multiscale (dark gray) force field.

systems²⁸ to reintroduce atomistic detail for the solvent molecules (see Methods). The behavior of the polymer and drugs over 5 ns of (fully atomistic) molecular dynamics (MD) was then examined. For comparison, the same configurations of the same subsystems were also simulated for 5 ns using the original multiscale parametrization. As discussed above, two particular features of the simulations that seemed to be important for influencing encapsulation efficiency were the density of the nascent nanoparticle and the orientational preferences of absorbed drug molecules. We evaluated the former by comparing the total radius of gyration of the nanoparticle in atomistic versus multiscale representations and the latter using the orientational metric described in the Methods section.

Since we were studying subsections from a larger simulation, taken at nonequilibrated periods, we expected that, even over 5 ns, the simulations would show some temporal evolution in the chosen metrics. At the same time, the confinement of the system within a much smaller periodic box meant that its behavior would probably differ to some extent from that observed in the parent simulation. The key test was that atomistic and multiscale subsystems should behave equivalently, as, indeed, was found to be the case (Figure 5). Changes from the initial configurations were minor, and the degree and rate of change in each parameter were very similar between atomistic and multiscale models. The simulations started at 30 ns showed the greatest relaxation, presumably because they began from configurations that were furthest from equilibrium (Figure 5).

Due to the short nature of these comparison simulations, we wanted to analyze the autocorrelation function to ascertain how relaxed the polymer was during the simulations (Figure 6).

Due to the limited number of data points and replicas, the curves are noisy, but it can be seen that, in general, the relaxation rates of the polymer chains are broadly similar in the multiscale and fully atomistic simulations.

Further Investigation of the Relative Dielectric Constant. To assess the effects of the relative dielectric constant (ϵ_r) on the multiscale simulation, we compared two additional multiscale simulations and one pure coarse-grain simulation against the 5 ns atomistic and multiscale simulations performed at the 50 ns time point (Figure 7A). Our original multiscale simulation uses $\epsilon_r = 6$; we tested the DXMP orientation and nanoparticle structure obtained using values of 1 and 15 and a pure coarse-grained model using $\epsilon_r = 15$.

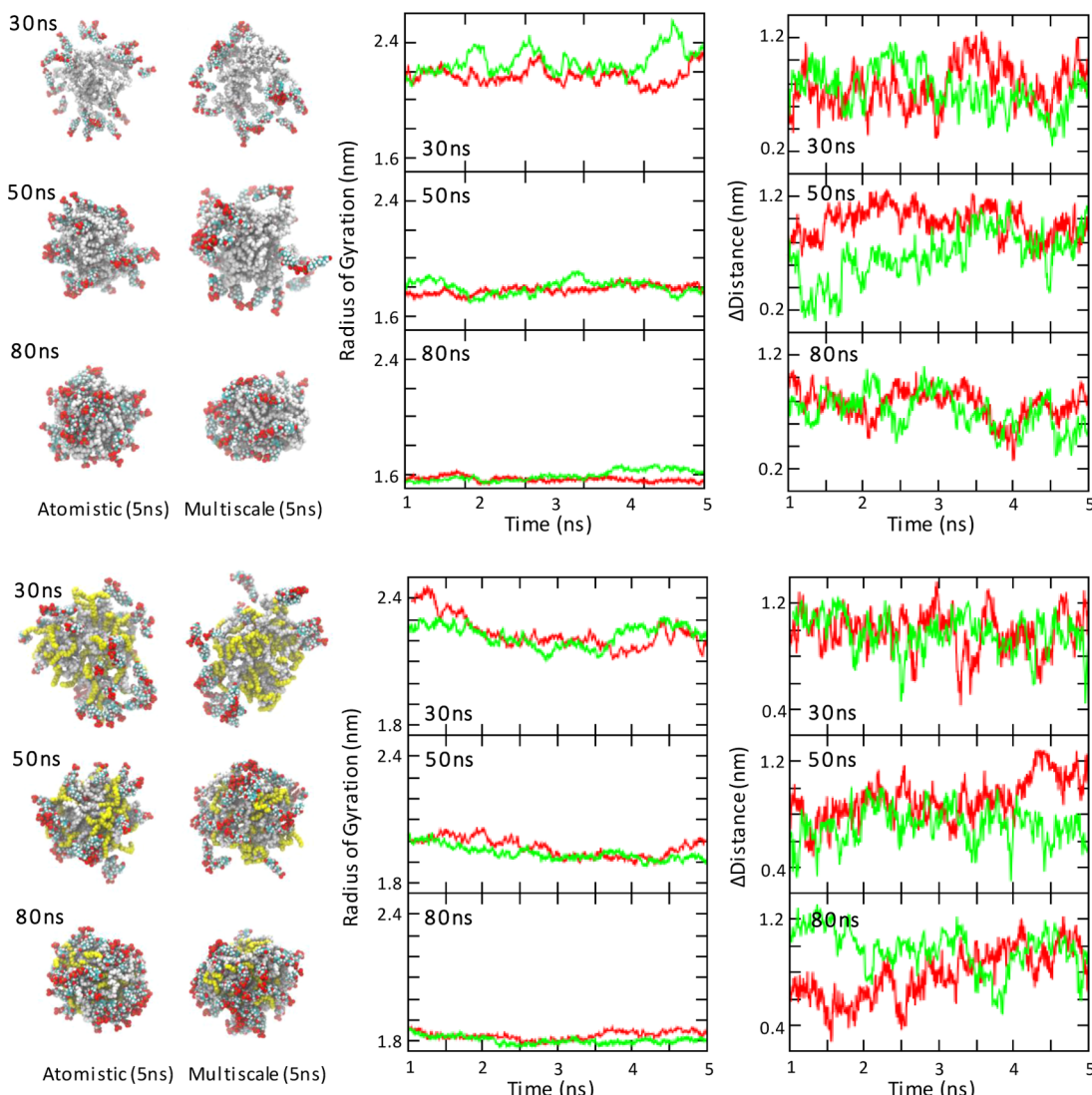


Figure 5. Analysis of PGA₁₀₀ (top) and PGA₂₀-co-C18PGA₈₀ (bottom) with DXMP. Left: Two snapshots from the end of the 5 ns simulations using both atomistic and multiscale force fields. DXMP (multi), PGA (white with C18 chains yellow). Graphs are shown for the total radius of gyration of the polymer cluster (middle) and the orientation of DXMP in relation to the center of mass of the polymer chains (right). Atomistic (red), multiscale (green).

With $\epsilon_r = 1$, the DXMP has an orientation almost the opposite of that found in the atomistic and original multiscale ($\epsilon_r = 6$) simulations. The phosphate head groups tend to be closer to the center of mass of the nanoparticle than the oxygen atoms at the tail end of the molecule. This is not unexpected because in the multiscale simulations the solvent is only modeled at the coarse-grained level and so does not have any electrostatic interactions. Our multiscale parametrization increases the coarse-grained phosphate–water nonbonded interactions, which leads to a better approximation of atomistic behavior. An increase of the dielectric constant to 15 allows the orientational preference of the absorbed drug to be predominantly maintained, but the reduction in the strength of all electrostatic interactions results in a generally flatter potential energy surface and orientational fluctuations become much more pronounced.

Perhaps surprisingly, the pure coarse-grained system, although lacking any atomistic solute–solute interactions, shows an orientation of DXMP that is very similar to that of the atomistic simulation, although with reduced fluctuations.

However, while this single metric seems to be well-satisfied, other aspects of the simulation are different from the atomistic standard, such as DXMP molecules aligning in an ordered crystal-like structure (Figure 7B). This result demonstrates the way in which the atomistic and coarse-grained aspects of a multiscale force field can interact in a complex way, which is challenging to predict.

Encapsulation Efficiency and Drug Loading. Experimentally, PGA₂₀-co-C18PGA₈₀ nanoparticles have shown a higher DXMP loading and encapsulation efficiency than those based on PGA.¹⁰ Our simulation results are in qualitative agreement with this trend: after running triplicates of both simulations, we found an increase in encapsulation efficiency and drug loading between these two polymers (Table 1).

To test our model further, we also simulated the encapsulation of DXMP by 100% C18 esterified PGA. Experimentally, a lower encapsulation efficiency is seen compared with that of PGA₂₀-co-C18PGA₈₀.¹⁰ We found that our model also confirmed this experimental trend with a reduction in encapsulation efficiency and drug loading for

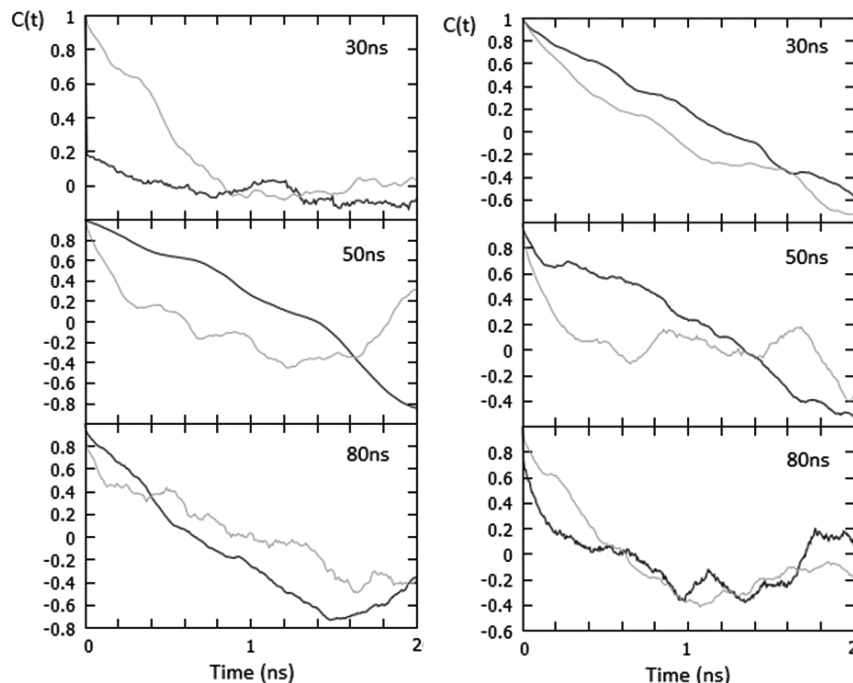


Figure 6. Autocorrelation function for PGA₁₀₀ (left) and PGA₂₀-co-C18PGA₈₀ (right) calculated using the radius of gyration for the polymer in Figure 4. Atomistic (dark gray), multiscale (light gray).

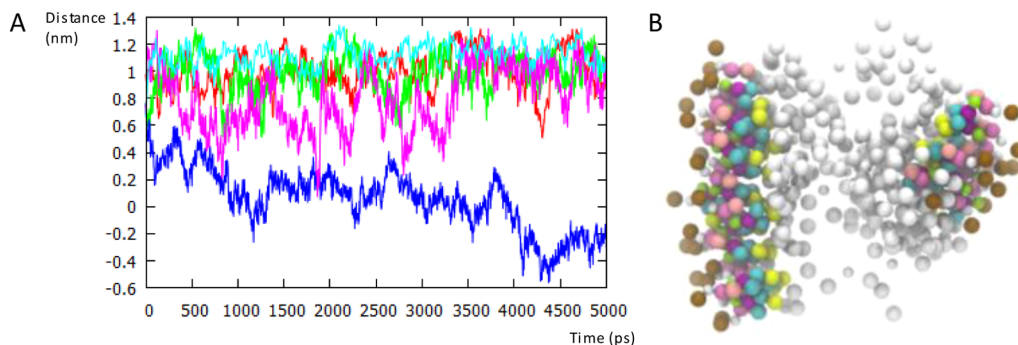


Figure 7. (A) Graph for the orientation of DXMP with respect to the polymer center of mass in five different systems. Atomistic (red), multiscale ($\epsilon_r = 6$) (green), multiscale ($\epsilon_r = 1$) (blue), multiscale ($\epsilon_r = 15$) (pink), coarse-grain ($\epsilon_r = 15$) (cyan). (B) Snapshot taken at the end of the coarse-grain simulation. PGA₂₀-co-C18PGA₈₀ (white), DXMP (multi), brown spheres represent the phosphate group of DXMP.

Table 1. Encapsulation Efficiency and Drug Loading for the Three Polymer Systems Calculated for Triplicate Repeats^a

	encapsulation efficiency (%)	% change from PGA ₁₀₀	drug loading (%)	% change from PGA ₁₀₀
PGA ₁₀₀	5.93 ± 0.25		44.76 ± 1.05	
PGA ₂₀ -co-C18PGA ₈₀	8.73 ± 0.25	+47.2	46.60 ± 0.71	+4.1
C18PGA ₁₀₀	6.07 ± 0.09	+2.4	34.16 ± 0.35	-23.7

^aData is obtained from the final snapshot of the simulation.

C18PGA₁₀₀ when compared with those of PGA₂₀-co-C18PGA₈₀ (Table 1).

The correlation between simulations and the experimental trends observed for drug incorporation provide mechanistic insight as to why PGA₂₀-co-C18PGA₈₀ is the most effective polymer at encapsulating DXMP. DXMP is amphiphilic ($\log P = 1.56$) and can interact favorably with both the organic and aqueous phases in the system. From our simulations, we observed that DXMP is surface-active, with multiple molecules positioned at the surface of the shrinking acetone drop. As the drop reduces in size, this brings the drug molecules toward the

surface of the aggregating polymer chains. This drives the interaction of DXMP with the polymer nanoparticle.

One advantage of using a computational model is that it can be quickly adjusted to test the new hypotheses. To further assess the effect of acetone dispersion on drug loading and encapsulation efficiency, we ran a simulation of PGA20-co-C18PGA80 with DXMP in pure water without acetone. The polymer and drug molar ratios were kept the same as those in the original multiscale simulation with acetone. We found a 23% reduction in the drug loading and 43% decrease in the encapsulation efficiency when compared to the original simulations using an acetone droplet.

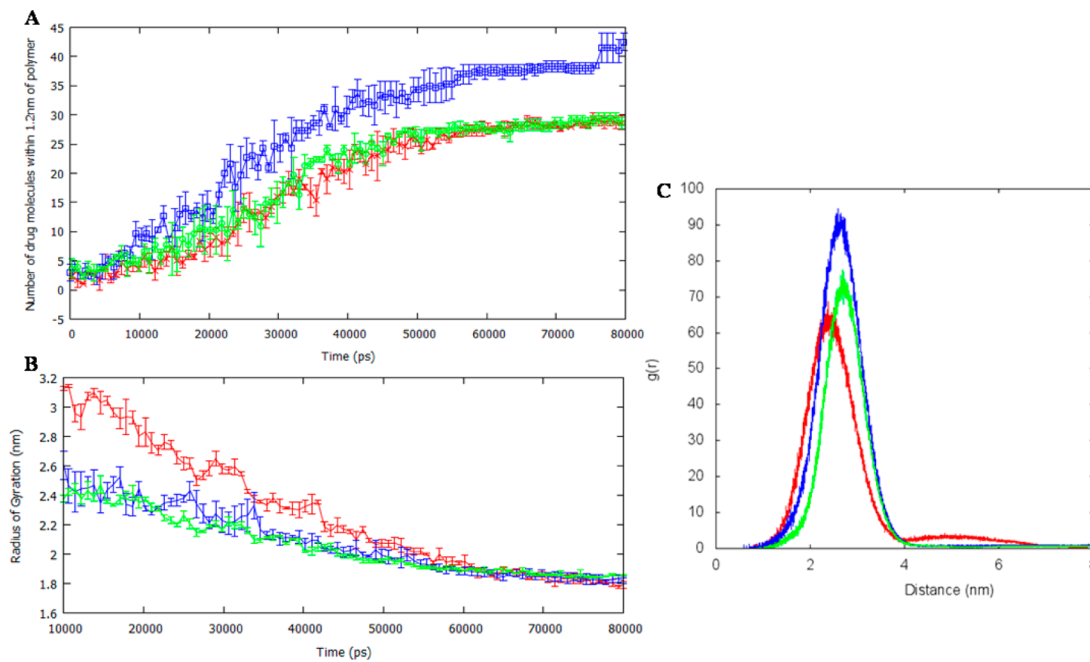


Figure 8. Metrics obtained from the 80 ns nanoprecipitation simulations: (A) number of DXMP molecules within 1.2 nm of the polymer chains, (B) radius of gyration of the all of the polymers during the 10–80 ns phase in the simulation, and (C) radial distribution functions of DXMP from the center of mass of the polymer during the last 30 ns of the simulation. Error bars are included (in A and B) for the standard error of the mean from triplicate repeats. PGA₁₀₀ (red), PGA₂₀-co-C18PGA₈₀ (blue), C18PGA₁₀₀ (green).

This result, albeit difficult to test experimentally, confirms our initial findings that acetone plays a major role in bringing drug molecules close to the surface of the polymer. A lack of acetone also results in faster polymer intermolecular collapse, which prevents the polymer chains from interacting with DXMP. It also indicates that a drug molecule benefits from having interactions with both the acetone and water, as this will allow the drug to be drawn toward the polymer as the acetone drop shrinks, increasing encapsulation efficiency and loading.

The positioning of DXMP at the acetone drop surface could also explain why experimental work shows that this drug is encapsulated better than cytarabine by these polymers.¹⁰ Cytarabine, with a log P of −2.8 and no charged groups, may not show affinity for the acetone/water interface and hence may not be pulled into the surface of the aggregating nanoparticle to the same extent as the acetone droplet shrinks.

The dispersion of acetone is consistent in all three systems, yet we see differences in encapsulation efficiency, i.e., the amount of drug that reaches the surface of the polymer nanoparticle. We analyzed the interaction of the polymer chains with the drug molecules over the course of the 80 ns simulations (Figure 8A). Specifically, we looked within the 1.2 nm cutoff for intermolecular interactions used in the simulations.

As the acetone drop disperses, DXMP molecules are brought within the 1.2 nm cutoff and they interact with the polymer chains. A saturation process is evident, and it is evident that PGA₂₀-co-C18PGA₈₀ is able to interact with more drug molecules than the other two polymers.

Calculating the radial distribution of DXMP around the center of mass of the polymer cluster during the last 30 ns of the nanoprecipitation simulations also revealed similar results (Figure 8B). The PGA₂₀-co-C18PGA₈₀ nanoparticle has a larger number of drug molecules surrounding it than PGA₁₀₀ or C18PGA₁₀₀.

To analyze these results further, the total radius of gyration (R_g) for all of the polymers was calculated during the 10–50 ns time period (Figure 8C). As acetone disperses, the polymer is exposed to water and this triggers the aggregation of the polymer chains. PGA₁₀₀ is most soluble in both acetone and water and so maintains the highest R_g during this time period. C18PGA₁₀₀ is the most hydrophobic polymer, and it compacts most quickly and most extensively. We conclude, therefore, that the optimal drug loading properties of PGA₂₀-co-C18PGA₈₀ are a result of a balance between the possibility of favorable, hydrophobic drug binding sites on the surface of the nanoparticle (favored by increasing levels of acylation) and the degree of collapse, and so effective surface area, of the nanoparticle (favored by decreased levels of acylation).

These results are in agreement with contact angle measurements on similar PGA polymers by Orafai et al.²⁹ A PGA₆₀-co-C8PGA₄₀ polymer showed the lowest surface free energy when compared with PGA₁₀₀ and C8PGA₁₀₀ polymers due to a balance of polar and nonpolar components.

CONCLUSIONS

A multiscale (dual resolution) modeling method has been used to simulate the encapsulation of DXMP by three related polymers. Detailed insights have been gained regarding the effects of acetone dispersion on the behavior and interactions of drug and polymer molecules. DXMP molecules are surface-active and show a preference for the retreating organic/aqueous interface of the dispersing drop of acetone. This results in the drug molecules being drawn toward the aggregating polymer chains within the shrinking acetone drop. An agreement with the experimental trend in encapsulation efficiency has been found for the three polymers tested. Our simulations show, while C18 chains are required to interact favorably with DXMP, having too many C18 chains decreases solubility, preventing the polymer from interacting with surrounding DXMP

molecules. A balance between hydrophobic and hydrophilic moieties in the polymer seems to be important for optimal drug incorporation.

In the absence of further experimental data to confirm details of our multiscale modeling, resolution transformation has been used to reintroduce atomistic detail to coarse-grained solvent. Fully atomistic simulations support the (relative) accuracy of the larger multiscale simulations.

Our success here and the relative simplicity of the multiscale modeling method has encouraged us to apply the approach to the simulation of new PGA derivatives with other small molecule drugs and should help to facilitate the design of more efficient PGA drug delivery systems in the future.

■ ASSOCIATED CONTENT

Supporting Information

Details of the coarse graining and all nonstandard force field parameters. The Supporting Information is available free of charge on the ACS Publications website at DOI: 10.1021/ct501152a.

■ AUTHOR INFORMATION

Corresponding Author

*E-mail: charles.laughton@nottingham.ac.uk. Tel.: +441159513405. Fax: +441159513412.

Funding

We would like to acknowledge the financial support from the EPSRC Centre for Doctoral Training and AstraZeneca, UK (grant no. EP/I01375X/1). C.A. thanks EPSRC for a Leadership Fellowship (grant no. EP/H005625/1X).

Notes

The authors declare no competing financial interest.

■ ACKNOWLEDGMENTS

Computing facilities were provided by the University of Nottingham HPC Service and HECToR, the UK National HPC Service.

■ REFERENCES

- (1) Wang, A. Z.; Langer, R.; Farokhzad, O. C. *Annu. Rev. Med.* **2012**, *63*, 185–198.
- (2) Kallinteri, P.; Garnett, M. Polymeric Nanoparticles for Drug Delivery. In *Nanotechnologies for the Life Sciences*; Kumar, C. S. S. R., Ed.; Wiley-VCH Verlag GmbH & Co. KGaA: Weinheim, Germany, 2007.
- (3) Mattheolabakis, G.; Rigas, B.; Constantinides, P. P. *Nanomedicine* **2012**, *7*, 1577–1590.
- (4) Ahmed, M.; Ramadan, W.; Rambhu, D.; Shakeel, F. *Pharmazie* **2008**, *63*, 806–811.
- (5) Carvalho, F. C.; Barbi, M. S.; Sarmento, V. H. V.; Chiavacci, L. A.; Netto, F. M.; Gremião, M. P. D. *J. Pharm. Pharmacol.* **2010**, *62*, 430–439.
- (6) Liu, J.; Xiao, Y.; Allen, C. *J. Pharm. Sci.* **2004**, *93*, 132–143.
- (7) Jeong, B.; Choi, Y. K.; Bae, Y. H.; Zentner, G.; Kim, S. W. *J. Controlled Release* **1999**, *62*, 109–114.
- (8) Vega, E.; Gamisans, F.; García, M. L.; Chauvet, A.; Lacoulonche, F.; Egea, M. A. *J. Pharm. Sci.* **2008**, *97*, 5306–5317.
- (9) Jelonek, K.; Kasperczyk, J.; Li, S.; Dobrzynski, P.; Jarzabek, B. *Int. J. Pharm.* **2011**, *414*, 203–209.
- (10) Puri, S.; Kallinteri, P.; Higgins, S.; Hutcheon, G. A.; Garnett, M. *C. J. Controlled Release* **2008**, *125*, 59–67.
- (11) Vauthier, C.; Bouchemal, K. *Pharm. Res.* **2009**, *26*, 1025–1058.
- (12) Galindo-Rodriguez, S.; Allermann, E.; Fessi, H.; Doelker, E. *Pharm. Res.* **2004**, *21*, 1428–1439.
- (13) Srinivas, G.; Discher, D. E.; Klein, M. L. *Nat. Mater.* **2004**, *3*, 638–644.
- (14) Fukunaga, H.; Takimoto, J.; Doi, M. *J. Chem. Phys.* **2002**, *116*, 8183.
- (15) Samanta, S.; Roccatano, D. *J. Phys. Chem. B* **2013**, *117*, 3250–3257.
- (16) Ahmad, S.; Johnston, B. F.; Mackay, S. P.; Schatzlein, A. G.; Gellert, P.; Sengupta, D.; Uchegbu, I. F. *J. R. Soc., Interface* **2010**, *7*, S423–33.
- (17) Loverde, S. M.; Ortiz, V.; Kamien, R. D.; Klein, M. L.; Discher, D. E. *Soft Matter* **2010**, *6*, 1419–1425.
- (18) Moeendarbary, E.; Ng, T. Y.; Zangeneh, M. *Int. J. Appl. Mech.* **2010**, *02*, 161–190.
- (19) Ortiz, V.; Nielsen, S. O.; Discher, D. E.; Klein, M. L.; Lipowsky, R.; Shillcock, J. *J. Phys. Chem. B* **2005**, *109*, 17708–17714.
- (20) Spaeth, J. R.; Kevrekidis, I. G.; Panagiotopoulos, A. Z. *J. Chem. Phys.* **2011**, *135*, 184903.
- (21) Hess, B.; Kutzner, C.; Van Der Spoel, D.; Lindahl, E. *J. Chem. Theory Comput.* **2008**, *4*, 435–447.
- (22) Marrink, S. J.; Risselada, H. J.; Yefimov, S.; Tieleman, D. P.; de Vries, A. H. *J. Phys. Chem. B* **2007**, *111*, 7812–7824.
- (23) Rzepiela, A. J.; Louhivuori, M.; Peter, C.; Marrink, S. J. *Phys. Chem. Chem. Phys.* **2011**, *13*, 10437–10448.
- (24) Wassenaar, T. A.; Ingólfsson, H. I.; Priess, M.; Marrink, S. J.; Schäfer, L. V. *J. Phys. Chem. B* **2013**, *117*, 3516–3530.
- (25) Bakowies, D.; Baron, R.; Christen, M.; Hu, P. H.; Geerke, D. P.; Heinz, T. I. M. N.; Kastenholz, M. A.; Gunsteren, W. F. V. A. N. *J. Comput. Chem.* **2005**, *7*, 1719–1751.
- (26) Malde, A. K.; Zuo, L.; Breeze, M.; Stroet, M.; Poger, D.; Nair, P. C.; Oostenbrink, C.; Mark, A. E. *J. Chem. Theory Comput.* **2011**, *7*, 4026–4037.
- (27) Rühle, V.; Junghans, C.; Lukyanov, A.; Kremer, K.; Andrienko, D. *J. Chem. Theory Comput.* **2009**, *5*, 3211–3223.
- (28) Wassenaar, T. A.; Pluhackova, K.; Böckmann, R. A.; Marrink, S. J.; Tieleman, D. P. *J. Chem. Theory Comput.* **2014**, *10*, 676–690.
- (29) Orafaai, H.; Kallinteri, P.; Garnett, M.; Huggins, S.; Hutcheon, G.; Pourcain, C. *Iran. J. Pharm. Res.* **2008**, *7*, 11–19.